

Collision process between an incident bead and a three-dimensional granular packing

Djaoued Beladjine, Madani Ammi, Luc Oger, and Alexandre Valance
Groupe Matière Condensée et Matériaux, UMR CNRS 6626, F-35042 Rennes cedex, France
 (Received 28 November 2006; published 14 June 2007)

We report on experimental studies of the collision process between an incident bead and a three-dimensional granular packing (made of particles identical to the impacting one). The understanding of such a process and the resulting ejection of particles is, in particular, crucial to describe eolian sand transport. We present here an extensive experimental analysis of the collision and ejection process. The analysis is two dimensional in the sense that we determined only the vertical component V_z of the ejection velocity of the splashed particles and the horizontal component V_x lying in the incident plane. We extracted in particular the distribution of the ejection velocities for a wide range of impact angles θ_i and incident velocity V_i . We show that the mean quadratic horizontal velocity of the splashed particles is almost insensitive to changes in the impact angle and velocity, while the mean quadratic vertical velocity slightly increases with increasing impact velocity (as $V_i^{1/2}$). Moreover, the mean number of splashed particles per collision is found to be dependent on both the impact angle and velocity, and to scale with the impact speed as $V_i^{3/2}$. A consequence of these outcomes is that the sum of the kinetic energy of the splashed particles is directly proportional to the kinetic energy of the incident particle. Finally, we provide the bivariate probability distribution function $P(V_x, V_z)$ of the ejection velocities and show that it can be approximated by the product of a log-normal distribution and a circular normal one.

DOI: [10.1103/PhysRevE.75.061305](https://doi.org/10.1103/PhysRevE.75.061305)

PACS number(s): 45.70.-n, 62.20.-x, 81.05.Rm

I. INTRODUCTION

Sand movement in deserts can cause damage to villages and seriously perturb the circulation on roads or railways. It is therefore crucial to understand the mechanisms of sand transport in order to stop or at least reduce it. Sand grains are lifted by the wind and accelerated during their flight. These highly energetic grains, called saltating grains, can travel over large distance by successive jumps [1,2]. As they impact the sand bed surface, they eject other grains from the bed. These splashed grains, termed reptating grains, contribute to the augmentation of the sand flux. Some of them can be promoted to the saltation motion. We are interested here in the collision process between a saltating grain and a packing of identical grains. We focused, in particular, on the energy redistribution through the rebound grain and the ejected grains. Note that air flow plays a negligible role in the collision process, since the latter lasts a very short time in comparison with the typical time scale of aerodynamics processes. This energy redistribution is described, in the literature, in terms of the splash function [2]. Previous experimental studies [3–5] provided interesting and valuable information, but the data remain usually sparse and the range of variation of the impact parameters (like the impact velocity, approach angle) are relatively limited. The difficulty comes from the fact that saltation is a stochastic process, and a great number of experiments is required to accumulate enough data for good statistics.

The splash process in eolian sand transport is connected in some way with the formation of impact craters. Recently, several studies focused on the morphology and size of impact craters formed in granular media [6,7]. The underlying physical mechanisms governing such processes are indeed of the same nature as those responsible for the splash. In addition, the formation of impact craters in granular media corresponds to a distinct collisional regime where the impacting

body is much more massive and larger than the particles of the impacted medium. In the saltation problem, the projectile and the target are composed of particles of the same nature and the regime of crater formation is never reached in the range of impact energy relevant for eolian transport. It is, however, interesting to note that craters can form at moderate impact energy in some particular configurations, as at the tip of a granular heap [8].

The present study aims at giving an extensive view of the splash function thanks to new data recently obtained from collision experiments between an incident bead and a three-dimensional (3D) granular packing made of particles identical to the impacting one. We varied the approach angle θ_i and the impacting speed V_i in a wide range ($10^\circ < \theta_i < 90^\circ$ and $50 < V_i/\sqrt{gd} < 200$, where d is the bead diameter and g the gravity acceleration) and analyzed the projection of the trajectories of the rebounding and splashed particles onto the incident plane $(0, x, z)$. We extracted in particular the distribution of the horizontal and vertical ejection velocities (V_x and V_z , respectively), and proposed laws for the variation of the mean horizontal and vertical ejection velocity as a function of the approach angle and impact velocity. We also determined the mean number of splashed particles and its evolution with the impact parameters. Lastly, we provided the bivariate probability distribution function $P(V_x, V_z)$ of the ejection speed of the splashed particles in the incident plane, and showed that it can be approximated by the product of a univariate log-normal distribution and a univariate circular normal one.

The paper is organized as follows. In Sec. II, we recall briefly the experimental and numerical results of the literature on the splash process. Section III describes the experimental setup used for the collision experiments. In Sec. IV, we present the experimental results concerning the rebound process of the incident bead, while Sec. V describes the features of the splashed grains. Finally, conclusions and perspectives are presented in Sec. VI.

II. EXPERIMENTAL AND NUMERICAL RESULTS IN THE LITERATURE

Several experimental studies focusing on the collision process have been conducted. Willets and Rice [3] observed collision phenomena with sand grains in wind tunnel experiments by means of high-speed video recordings. They found that the impacting grains hit the sand surface at small angles between 10° and 16° and rebounded with an angle between 20° and 40° . In addition, they established that the grains ejected from the granular bed have an average speed of one order of magnitude less than the impact speed.

In parallel, model experiments of collisions between an incident bead and a granular packing have been performed by different authors. Mitha *et al.* [4] studied the collision between a steel bead and a three-dimensional packing of steel beads. Beads of 4 mm diameter were used and the impacting bead was launched at a speed of 20 m/s. They investigated essentially the influence of the impact angle on the collision process. The mean normal restitution coefficient for the impacting bead, defined as the ratio between the vertical rebound speed and the vertical incident speed, was found to decrease with increasing impact angle ($\bar{e}_z=0.7$ at 17° and $\bar{e}_z=0.3$ at 31°). Furthermore, they showed that the number of ejected beads does not vary significantly when the impact angle increases from 17° to 31° , and that the average vertical speed of ejection is on the order of $3\sqrt{gd}$. Werner [5] also studied extensively the collision process for shallow impact angles. He used sand grains and designed a special apparatus to propel a sand grain with a given velocity. He found in particular that the normal restitution coefficient for the impact grain is independent of the incident speed ($\bar{e}_z=0.82$ at 15°). He observed in addition that the number of ejected grains increases with increasing incident speed and that the distribution of the vertical ejection velocity is nearly independent of the incoming velocity.

More recently, Rioual *et al.* [9–11] designed a two-dimensional setup to investigate the collision between a 6-mm-diameter incident bead and a two-dimensional granular packing of identical beads confined between two parallel vertical glass walls. This study confirmed Werner's observations [5]: the normal restitution coefficient for the impacting bead is independent of the impact speed, and the mean number of ejected grains varies nearly linearly with the impact speed. However, Rioual *et al.* [11] found that the mean vertical ejection velocity V_z increases slightly with increasing incident speed (i.e., roughly as the square root of the incident speed: $\bar{V}_z \sim V_i^{1/2}$) and proposed the following law for the decreasing part of the probability distribution function of the vertical ejection velocities [10]:

$$P(V_z) = \frac{V_z}{\sigma^2} \exp\left(-\frac{V_z^2}{2\sigma^2}\right), \quad (1)$$

where $\sigma^2=0.1V_i\sqrt{gd}$. This law is known as the Rayleigh distribution.

In addition to experiments, numerical simulations of the collision process have been performed by several authors [12–15]. Most of these studies were restricted to a two-dimensional configuration except in [15]. We find it worth-

while to recall the significant outcomes of the numerical studies. Werner [5,12] made 2D simulations of the collision process between a sphere and an ordered packing of spheres by means of a discrete element method. The outcomes of his simulations were found to be in agreement with his experimental results obtained with sand grains of 800 μm diameter. In particular, he was able to extract a law for the mean vertical speed amplification \bar{e}_z of the rebound particle, which was found to be independent of the impact speed:

$$\bar{e}_z(\theta_i) = \left(\frac{0.320}{\sin \theta_i} - 0.236\right) \bar{e}_z(15^\circ) = \frac{0.262}{\sin \theta_i} - 0.193, \quad (2)$$

where θ_i is the impact angle measured with respect to the horizontal and $\bar{e}_z(15^\circ)=0.82$. He also established a law for the mean number \bar{n}_{ej} of ejected particles as a function of the incident angle and speed:

$$\begin{aligned} \bar{n}_{ej}(\theta_i, V_i) &= 3.36 \sin \theta_i (0.572 V_i - 0.915) \\ &= 3.07 \sin \theta_i \left(\frac{V_i}{18\sqrt{gd}} - 1\right). \end{aligned} \quad (3)$$

Lastly, he pointed out the importance of the geometry of the packing surface for the ejection process, and suggested that the bivariate probability distribution of the ejection speed can be approximated by the product of a Rayleigh distribution for V_z and a normal one for V_x :

$$P(V_x, V_z) = \frac{V_z}{\sqrt{2\pi}\sigma^3} \exp\left(-\frac{V_x^2 + V_z^2}{2\sigma^2}\right) \quad (4)$$

with $\sigma \approx 3.4\sqrt{gd}$. Anderson and Haff [13,14] also performed extensive simulations of the collision of spherical bead onto a two-dimensional disordered packing. They investigated the influence of the impact velocity on the ejection process for shallow impacting angles (8° and 11°) and spherical grains of 230 μm diameter. They found that the mean number of ejected grains scales as

$$\bar{n}_{ej}(V_i) = 1.75 V_i = V_i/12\sqrt{gd}, \quad (5)$$

and that the distribution of the 2D ejection speed V_{xz} ($V_{xz} = \sqrt{V_x^2 + V_z^2}$) can be fitted by an exponential law of the form

$$P(V_{xz}) = \frac{1}{0.25V_i^{0.3}} \exp\left(-\frac{V_{xz}}{0.25V_i^{0.3}}\right). \quad (6)$$

The latter result leads to a mean ejection speed scaling as

$$\bar{V}_{xz} = 0.25V_i^{0.3} = 0.73\sqrt{gd} \left(\frac{V_i}{\sqrt{gd}}\right)^{0.3}. \quad (7)$$

The scaling exponent is quite close to that obtained by Rioual for the vertical ejection speed [10].

III. EXPERIMENTAL SETUP AND IMAGE ANALYSIS

A. Experimental setup

We used PVC beads of 6 mm diameter and 0.2 g mass. The incident particle and those of the packing are identical. The friction and normal restitution coefficients of the bead

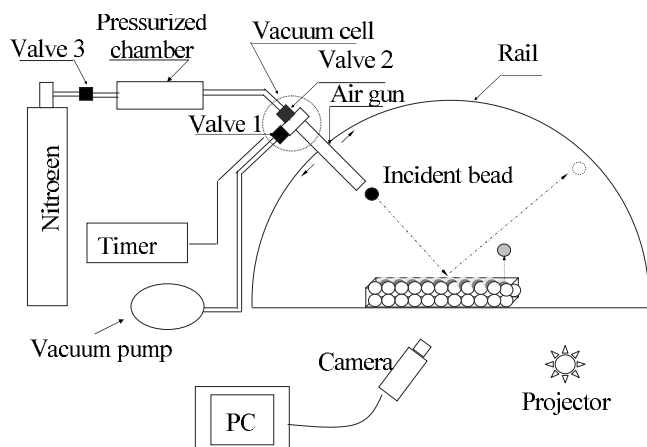


FIG. 1. Experimental setup.

are, respectively, $\mu=0.19$ and $\varepsilon=0.91$. The experimental setup is shown in Fig. 1. An air gun was designed to propel a single bead onto the packing. By varying the pressure, the incident speed can be adjusted to a given value within a certain range (see [9] for a detailed description). The air gun can move on a semicircular rail which allows the incident angle to be varied from 0° to 90° . The packing is built by displaying randomly the beads in a square box of dimension $42 \times 42 \times 23 \text{ cm}^3$. The packing fraction is on the order of 0.6.

The collision process is recorded via a fast video camera which takes up to 500 images per second. The video camera was placed perpendicularly to the incident plane.

B. Image analysis

The consecutive images of the collision (see Fig. 2) were processed to extract the kinematic properties of the incident bead and the ejected ones. The procedure was as follows. By means of an image analysis software, the positions of the splashed beads were determined on each image, then the trajectories of all ejected particles were reconstructed. As indicated above, we analyzed the trajectories of the splashed beads in the incident plane and had therefore access to the vertical velocity V_z and the horizontal component V_x in the

incident plane. The free surface of the packing was leveled before each collision experiment.

Furthermore, one should point out that the identification of the ejected beads is delicate in the first stages of the ejection process, since they are not clearly detached from the bed. As a consequence, we were able to identify the ejected beads only if they reached a height greater than one bead diameter above the bed. It means that we did not take into account, in our analysis, the weakly energetic beads which have a vertical ejection speed smaller than $V_0 = \sqrt{2gd}$.

C. Pertinent dimensionless variables

In our model, we used particles of much greater diameter than that of sand grains transported by the wind. Saltating sand grains in deserts have a diameter between 100 and 200 μm . One of the pertinent parameters characterizing the collision process for monodisperse particles is the Froude number: $\text{Fr} = V_i / \sqrt{gd}$. In standard conditions of sand transport in deserts and for sand grains of 200 μm , the impact velocities of the saltating grains range from 2 to 10 m/s. The Froude number lies therefore between 50 and 250. Using 6-mm-diameter beads, we have to work with impact speeds ranging from 10 to 50 m/s in order to reach such values for the Froude number.

D. Impact parameters

We present here experimental results about the collision process when the incident speed and the impact angle are varied. The impact angles were measured with respect to the horizontal plane. We made three series of experiments: one at a given incident velocity of 26 m/s with impact angles ranging from 10° to 90° , and two other ones at a fixed impact angle (10° and 40° , respectively) with incident speeds ranging from 18 to 40 m/s (see Table I). To obtain good statistics, we carried out about 100 collisions for each set of impact parameters (i.e., angle and velocity).

IV. EXPERIMENTAL RESULTS: PROPERTIES OF THE REBOUNING BEAD

A typical collision is characterized by a rebounding particle and a set of splashed particles. The rebound bead has a

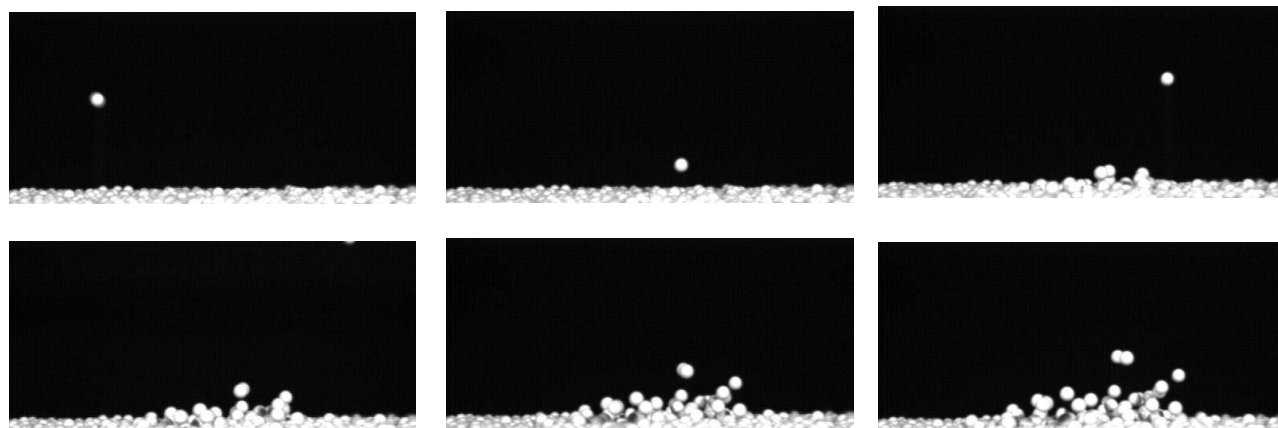


FIG. 2. Successive snapshots of the collision. The time step between two successive images is 4 ms.

TABLE I. Impact parameters investigated experimentally. For each set of parameters, about 100 collision experiments were achieved.

	V_i (m/s)						
	18	20	22	24	26	29	39
	$Fr = V_i / \sqrt{gd}$						
θ_i	74	82	91	99	107	120	161
10°	×	×	×	×	×	×	×
20°					×		
40°	×				×		×
60°					×		
90°					×		

much larger speed than that of the splashed beads. We analyzed the effect of both the incident angle and speed on the rebound particle. In this analysis, we extracted the 2D rebound velocity $V_{r,xz}$ and the 2D rebound angle θ_r (see Fig. 3 for its definition).

Figure 4 displays the variation of the mean rebound angle $\bar{\theta}_r$ as a function of the impact angle and the incident speed. The rebound angle appears to be independent of the incident speed, while it increases with increasing impact angle. The rebound is not specular (i.e., $\theta_r \neq \theta_i$). The experimental results show that, at grazing angles, the rebound angle is greater than the incident angle, whereas, for impact angles higher than 20°, the rebound angle is less than the incident one. For an impact angle of 10°, which is a typical value for saltating grains, the mean rebound angle is found to be $22^\circ \pm 10^\circ$. The data can be fitted reasonably well by a rational function of $\sin \theta_i$:

$$\sin \bar{\theta}_r = \frac{A_z - B_z \sin \theta_i}{A - B \sin \theta_i}. \quad (8)$$

The best fit gives $A_z=0.30$, $B_z=0.15$, $A=0.87$, and $B=0.72$.

For the analysis of the rebound velocity, we introduce two different coefficients of restitution: $e_z = V_{rz}/V_{iz}$ and e_{xz}

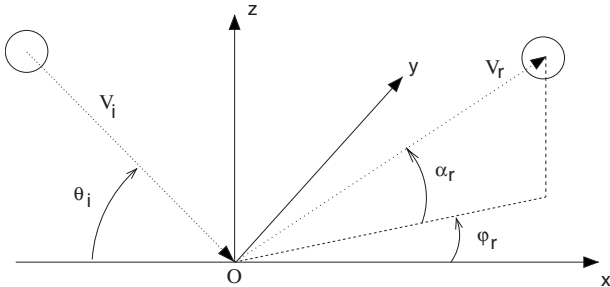


FIG. 3. Definition of the rebound angles α_r and φ_r . The impacting particle lies in the vertical plane $(0, x, z)$ and hits the bed with an incident angle θ_i . α_r is the angle between the horizontal plane and the rebound velocity V_r , whereas φ_r is the angle between the Ox axis and the projection of the rebound velocity onto the horizontal plane. We also define the 2D rebound angle θ_r as the angle between the Ox axis and the projection of the rebound velocity onto the incident plane $(0, x, z)$: $\tan \theta_r = \tan \alpha_r / \cos \varphi_r$.

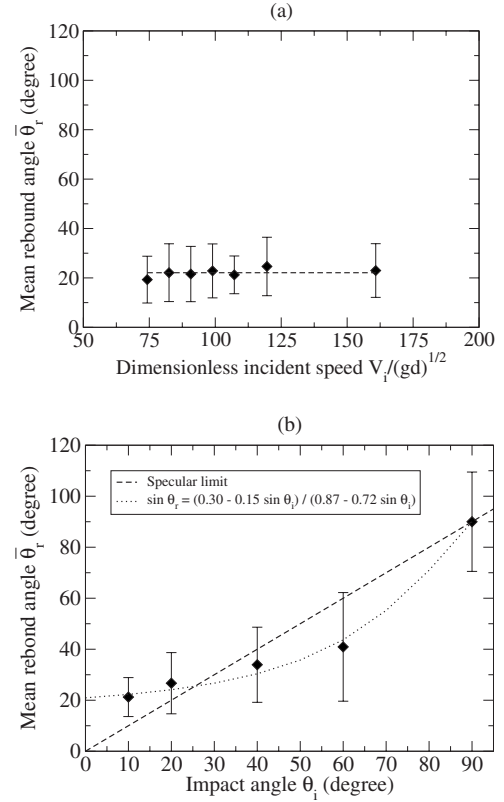


FIG. 4. Variation of the mean rebound angle $\bar{\theta}_r$ (a) versus the incident speed at a given incident angle $\theta_i=10^\circ$; (b) versus the impact angle at a given incident speed $V_i=26$ m/s $\approx 107\sqrt{gd}$. In (b), the dashed line represents the specular limit (i.e., $\theta_r=\theta_i$), whereas the dotted line is the best fit of the form given by Eq. (8).

$=V_{r,xz}/V_i$, where V_i and $V_{r,xz}$ are, respectively, the incident and the rebound velocity in the incident plane $(0, x, z)$, and V_{iz} and V_{rz} correspond to their vertical components.

We plotted, in Fig. 5(a), the mean restitution coefficients \bar{e}_z and \bar{e}_{xz} as a function of the incident velocity. No significant variation of the restitution coefficients is observed within the range of impact velocity investigated so far. This independence of the incident velocity was also found in 2D collision experiments [9] and 3D ones with sand grains [5].

Figure 5(b) shows the evolution of the mean restitution coefficients \bar{e}_z and \bar{e}_{xz} versus the impact angle for a given incident speed of 26 m/s. The mean restitution coefficients \bar{e}_z and \bar{e}_{xz} decrease with increasing impact angle. The data can be relatively well fitted by laws of the following forms:

$$\bar{e}_z = \frac{A_z}{\sin \theta_i} - B_z, \quad (9)$$

$$\bar{e}_{xz} = A - B \sin \theta_i, \quad (10)$$

with $A_z=0.30$, $B_z=0.15$, $A=0.87$, and $B=0.72$. Note that the values of the coefficients A , B , A_z , and B_z are identical to those found in Eq. (8). For \bar{e}_z , the same type of law was proposed by Werner [5]. If we reformulate Eq. (9) in the same terms as Werner, we find $\bar{e}_z = (0.3/\sin \theta_i - 0.15)\bar{e}_z(15^\circ)$. The numerical constants are slightly different from those of

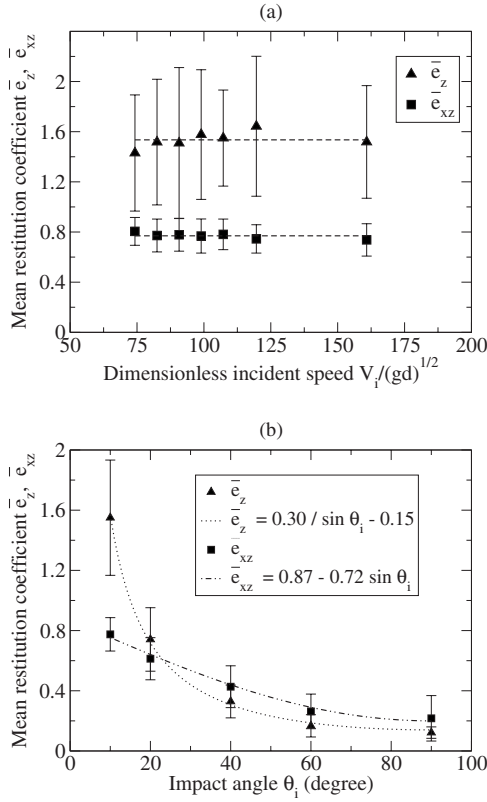


FIG. 5. Variation of the mean restitution coefficients \bar{e}_z and \bar{e}_{xz} (a) versus the impact speed V_i at a given incident angle $\theta_i = 10^\circ$; (b) versus the impact angle θ_i at a given incident speed $V_i = 26$ m/s. In (a), the horizontal dashed lines correspond to an average of the data. In (b), the dotted lines stand for best fits of the form $A_z/\sin \theta_i - B_z$ for e_z (with $A_z = 0.30$ and $B_z = 0.15$), and $A - B \sin \theta_i$ for e_{xz} (with $A = 0.87$ and $B = 0.72$).

Werner [cf. Eq. (2)] and this discrepancy may be due to the fact that the PVC beads do not have the same mechanical properties as those of the quartz sand grains.

It is sometimes useful to characterize the rebound process in terms of energy loss. The average fraction of energy lost by the incident bead is $(1 - \bar{e}_{xz}^2) = (1 - \bar{e}_z^2 - \sigma^2)$, where σ^2 is the variance of the restitution coefficient e_{xz} . σ^2 is found, to first order, independent of the impact angle and velocity, and most importantly is rather small: $\sigma^2 \approx 0.02$. The error made, when approximating $(1 - \bar{e}_{xz}^2)$ by $(1 - \bar{e}_z^2)$, is therefore negligible. Lastly, one can note that the rebound angle θ_r can be expressed in terms of e_z and e_{xz} as

$$\overline{\sin \theta_r} = \overline{(e_z/e_{xz})} \sin \theta_i \approx (\bar{e}_z/\bar{e}_{xz}) \sin \theta_i. \quad (11)$$

Using Eqs. (9) and (10), it is straightforward to show that we obtain the same expression as that given by Eq. (8).

Additional comments follow. First, the incident bead loses much more energy for normal impacts [$\bar{e}_{xz}(90^\circ) = 0.22$] than for grazing ones [$\bar{e}_{xz}(10^\circ) = 0.78$]. Second, the vertical restitution coefficient e_z is found to exceed unity for grazing angles [$\bar{e}_z(10^\circ) = 1.55$]. This result does not violate energy conservation (since \bar{e}_{xz} is always smaller than 1) but simply means that a great part of the horizontal momentum of the

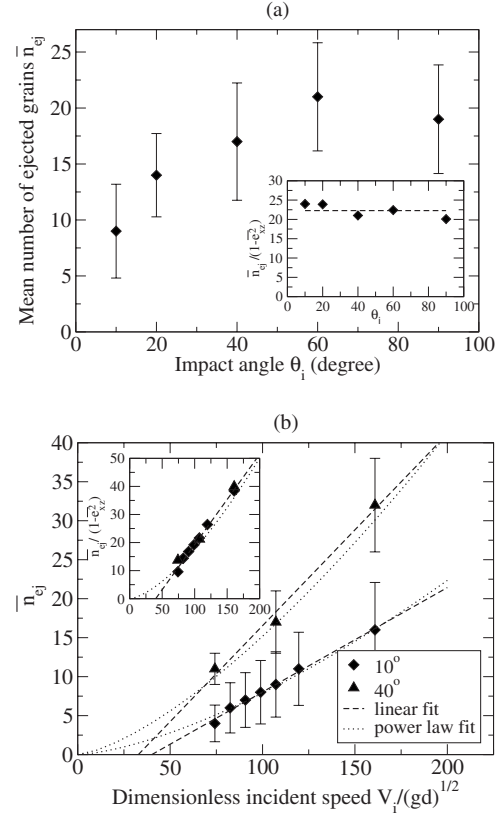


FIG. 6. Mean number of ejected beads (a) versus the impact angle θ_i for a given incident speed of 26 m/s; (b) versus the impact speed for an impact angle of 10° (\blacklozenge) and 40° (\blacktriangle).

incident particle is transferred to the vertical direction after the impact. In the context of the eolian transport of sand, this last result is of significant importance. Indeed, the sand grains transported by the wind in the desert have grazing impact angles between 8° and 15° [1,16,17]. This means that the latter will be able to rebound at a height at least equivalent to that before the collision. As a consequence, the grains will be able to continue their saltation process.

V. EXPERIMENTAL RESULTS: PROPERTIES OF THE EJECTED BEADS

When the incident bead impacts the bed, it not only rebounds but can also eject other beads from the packing. The ejected beads fly off in all directions with a speed which rarely overcomes 10% of the incident velocity. We present below the features of the ejected beads when the impacting angle and incident velocity are varied.

A. Number of ejected beads

Figure 6(a) displays the mean number of ejected beads per collision as a function of the impact angle at a given impact speed of 26 m/s. The mean number of ejected beads \bar{n}_{ej} increases with increasing impact angle. If we renormalize the mean number of splashed particles by $(1 - \bar{e}_{xz}^2)$, we surprisingly find a constant value. We recall that $(1 - \bar{e}_{xz}^2)$ represents the fraction of the kinetic energy of the incident particle

communicated to the packing. \bar{n}_{ej} can therefore be written as

$$\bar{n}_{ej}(\theta_i, V_i) = f(V_i)(1 - \bar{e}_{xz}^2), \quad (12)$$

where f is a function of V_i to be determined. For $V_i = 26$ m/s, one finds $f \approx 22$.

At a fixed impact angle, the average number of ejected beads also increases monotonically with increasing impact speed [see Fig. 6(b)]. The data for impact angles of 10° and 40° can be well fitted by a linear law of the form

$$\bar{n}_{ej}(\theta_i, V_i) = h(\theta_i) \left(\frac{V_i}{V_{ic}} - 1 \right). \quad (13)$$

h is a function of θ_i . V_{ic} can be interpreted as a threshold impact velocity below which there is no splashed grains and depends *a priori* on the impact angle θ_i . For $\theta_i = 10^\circ$, $h \approx 5.4$ and $V_{ic} \approx 40\sqrt{gd}$, and for $\theta_i = 40^\circ$, $h \approx 8.1$ and $V_{ic} \approx 34\sqrt{gd}$. It turns out that the critical velocity V_{ic} is not too sensitive to the impact angle, whereas h strongly varies with the impact angle. Renormalizing the mean number of ejected grains by $(1 - \bar{e}_{xz}^2)$, all data collapse on a single straight line whose equation is given by

$$\bar{n}_{ej} \approx 13.0(1 - \bar{e}_{xz}^2) \left(\frac{V_i}{40\sqrt{gd}} - 1 \right). \quad (14)$$

It is worthwhile noting that Eq. (14) is different from that suggested by Werner [cf. Eq. (3)]. Indeed, we found that $(1 - \bar{e}_{xz}^2) \approx (1 - A^2) + 2AB \sin \theta_i - B^2 \sin^2 \theta_i$, and therefore the dependence of \bar{n}_{ej} on θ_i is here more complicated than a simple linear law with $\sin \theta_i$, as proposed by Werner.

Finally, we would like to stress that it is difficult from the experiments to determine the threshold impact speed. First, the counting of the low-energy ejected particles is very sensitive to the accuracy of the experimental procedure used to detect the particles and to the definition of an ejected particle. We recall that we were able to detect with a good accuracy only particles ejected with a vertical velocity greater than $\sqrt{2gd}$. Second, at low impact velocity, the probability to observe a collision with a number of ejecta greater than or equal to 1 becomes very low, and a great number of experiments is therefore required to get a relatively good accuracy in the determination of \bar{n}_{ej} . As a consequence, we have no experimental means to check whether the threshold impact speed is really finite, as expected from the extrapolation of the linear fits.

If we deny the existence of a finite threshold impact speed, or, in other words, if we assume that the mean number of ejected grains is reduced to zero only for vanishing impact velocity, we can be tempted to fit the data by a power law. The best power law fit gives

$$\bar{n}_{ej} = 0.02(1 - \bar{e}_{xz}^2) \left(\frac{V_i}{\sqrt{gd}} \right)^{2-\alpha}, \quad (15)$$

with $\alpha \approx 0.5$. The exponent is not far from 2, which is the expected value if the number of ejected particles is proportional to the incident kinetic energy. We will see in the following sequel that \bar{n}_{ej} scales in fact as V_i^2/V_{xz}^2 (where V_{xz}^2 is the

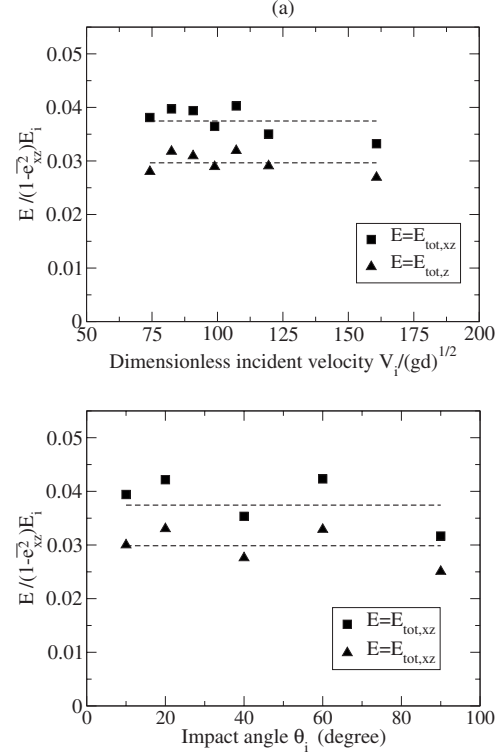


FIG. 7. Sum of the kinetic energy of the splashed beads in a collision process (a) versus the impact velocity at a fixed impact angle of 10° ; (b) versus the impact angle at a fixed impact speed of 26 m/s. The dashed lines represent an average of the data.

2D mean quadratic velocity of the ejected particles) and that V_{xz}^2 is found to vary as V_i^α .

B. Total kinetic energy of the ejected beads

We extracted from our data the total 2D kinetic energy $E_{tot,xz}$ of the ejected beads in a collision process (see Fig. 7). We renormalized $E_{tot,xz}$ by the fraction of energy communicated to the granular bed, that is $(1 - \bar{e}_{xz}^2)E_i$ where $E_i = mV_i^2/2$. The dimensionless kinetic energy $E_{tot,xz}/(1 - \bar{e}_{xz}^2)E_i$ is found to be rather independent of the incident speed and impact angle. Its value fluctuates between 0.03 and 0.04, and can be assumed to first order to be a constant, denoted later on by r . The value of r may depend on the mechanical properties of the bead. With the PVC beads used in the experiments, we get $r \approx 0.038$. This result shows that, at a fixed impact angle, the sum of the kinetic energy of the ejected grains is proportional to the kinetic energy of the incident bead (since \bar{e}_{xz} is independent of V_i) and that, at a fixed impact velocity, $E_{tot,xz}$ increases with increasing impact angle (since \bar{e}_{xz} decreases with increasing impact angle θ_i).

We also find that the vertical dimensionless kinetic energy $r_z = E_{tot,z}/(1 - \bar{e}_{xz}^2)E_i$ is also insensitive to the impact speed and impact angle (see again Fig. 7). With our PVC beads, this energy ratio is found to be $r_z \approx 0.030$.

C. Distributions of the vertical and horizontal ejection speeds

We analyzed the vertical and horizontal velocity distribution of the ejected beads. The distribution of the vertical

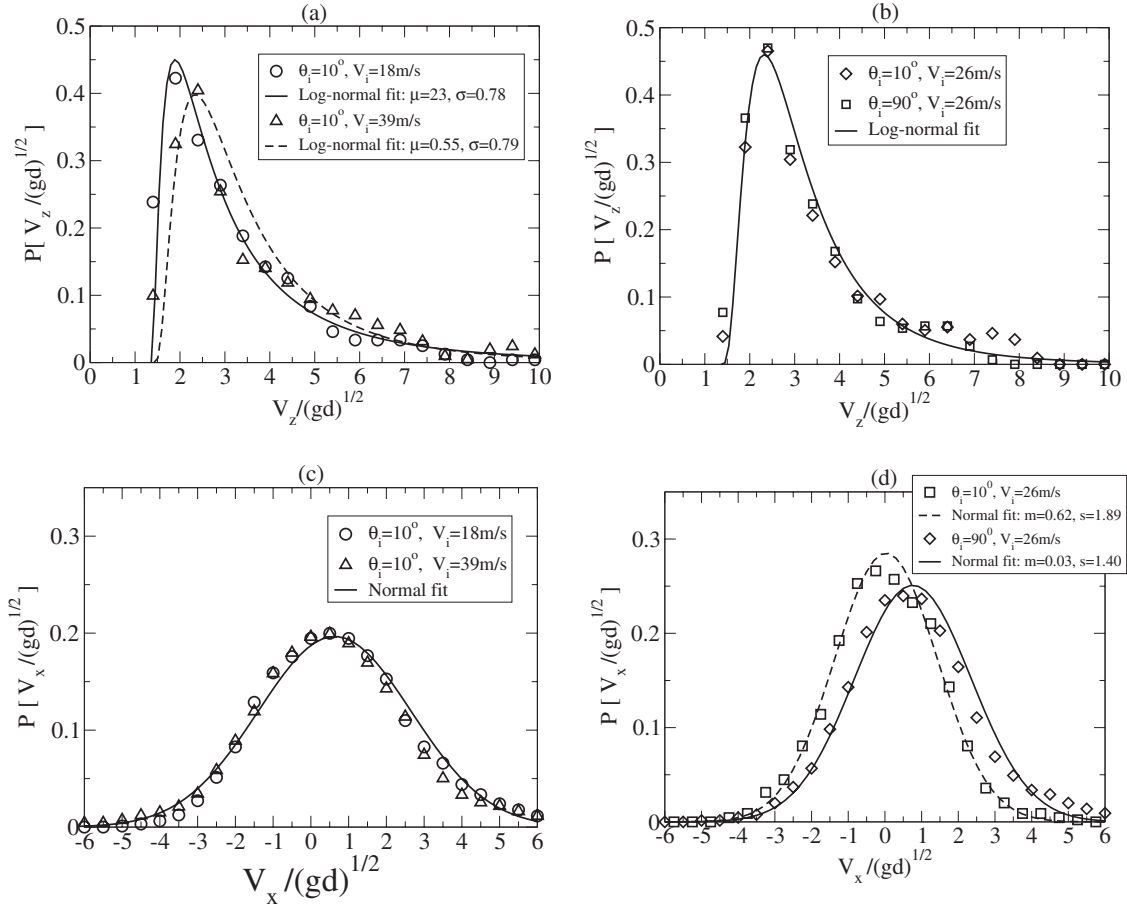


FIG. 8. Distribution of the vertical and horizontal ejection velocities (a) and (c) for various impact speeds at a fixed impact angle of 10° ; (b) and (d) for various impact angles at a fixed impact velocity of 26 m/s. The continuous lines represent the corresponding log-normal distributions [in (a) and (b)] and normal ones [in (c) and (d)].

recoil speeds for various impact speeds and impact angles are displayed in Figs. 8(a) and 8(b). All the distributions can be extremely well approximated by a log-normal law of the form

$$P[\tilde{V}_z] = \frac{1}{\sqrt{2\pi\sigma}(\tilde{V}_z - \tilde{V}_0)} \exp\{-[\ln(\tilde{V}_z - \tilde{V}_0) - \mu]^2/2\sigma^2\} \quad (16)$$

where $\tilde{V}_z = V_z/\sqrt{gd}$ and $\tilde{V}_0 = \sqrt{2}$. We recall that \tilde{V}_0 is the dimensionless critical ejection velocity below which we could not detect the splashed particles. The distribution is therefore truncated for low ejection speeds. The parameters μ and σ characterize the log-normal distribution and are determined as follows:

$$\mu = \overline{\ln(\tilde{V}_z - \tilde{V}_0)} = \ln[\overline{(\tilde{V}_z - \tilde{V}_0)^2}/\overline{(\tilde{V}_z - \tilde{V}_0)^2}], \quad (17)$$

$$\sigma^2 = \overline{[\ln(\tilde{V}_z - \tilde{V}_0)]^2} - \mu^2 = \overline{\ln[(\tilde{V}_z - \tilde{V}_0)^2/(\tilde{V}_z - \tilde{V}_0)^2]}. \quad (18)$$

The values of μ and σ have been calculated for various impact angles and velocities (see Table II). The result obtained here for the distribution of the vertical ejection veloci-

TABLE II. Main features of the distributions of the horizontal and vertical ejection speed, for various impact speeds at a fixed impact angle of 10° , and for various impact angles at a fixed impact velocity $V_i=26$ m/s. We recall that s corresponds to the root mean square of the horizontal velocity, and μ and σ are the parameters of the log-normal distribution of $(V_z - V_0)/\sqrt{gd}$ [see Eqs. (17) and (18)].

V_i (m/s)	$\bar{V}_x/\sqrt{gd}=m$	\bar{V}_x^2/gd	s	\bar{V}_z/\sqrt{gd}	\bar{V}_z^2/gd	μ	σ
18	0.85	4.41	1.92	3.12	12.24	0.23	0.78
20	0.82	3.34	1.64	3.22	13.39	0.26	0.81
22	0.77	3.65	1.75	3.21	13.38	0.25	0.82
24	0.77	3.54	1.72	3.25	13.59	0.29	0.80
26	0.62	3.94	1.89	3.41	15.08	0.38	0.79
29	0.86	3.47	1.65	3.61	16.90	0.49	0.77
39	0.63	4.50	2.03	3.79	19.24	0.55	0.79
θ_i	$\bar{V}_x/\sqrt{gd}=m$	\bar{V}_x^2/gd	s	\bar{V}_z/\sqrt{gd}	\bar{V}_z^2/gd	μ	σ
10°	0.62	3.94	1.89	3.41	15.08	0.38	0.79
20°	0.49	2.32	1.44	3.28	12.69	0.40	0.67
40°	0.41	2.24	1.44	3.22	12.06	0.39	0.64
60°	0.38	2.58	1.56	3.40	13.49	0.48	0.63
90°	0.03	1.95	1.40	3.15	11.47	0.34	0.65

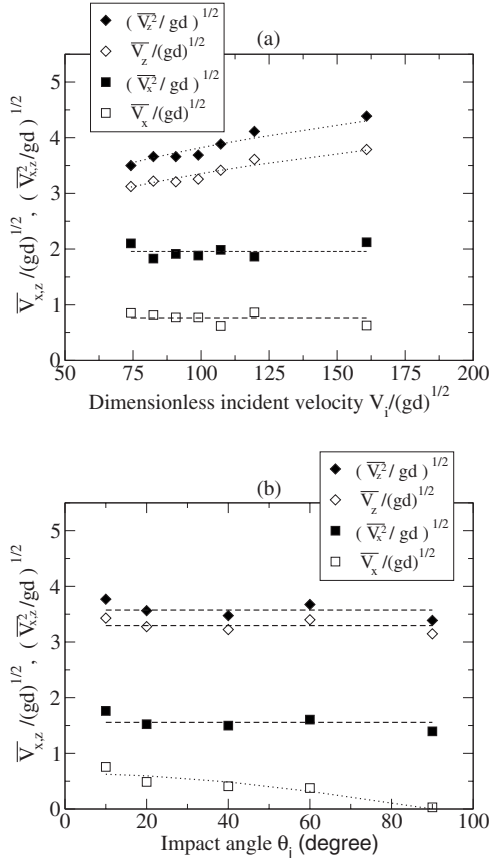


FIG. 9. Mean vertical and horizontal ejection velocities (\bar{V}_z , \bar{V}_x) and mean corresponding quadratic velocities ($(\bar{V}_z^2/gd)^{1/2}$, $(\bar{V}_x^2/gd)^{1/2}$) (a) versus the impact speed at a fixed impact angle of 10° ; (b) versus the impact angle at a fixed impact velocity $V_i=26$ m/s. The horizontal dashed lines correspond to an average of the data while the dotted lines stand for fits of the following form: $\bar{V}_z \sim (\bar{V}_z^2/gd)^{1/2} \sim V_i^{1/4}$ and $\bar{V}_x \sim \cos \theta_i$.

ties is different from that found by Rioual *et al.* [10] and Werner [5]. We recall that they got a Rayleigh distribution [cf. Eqs. (1) and (4)]. The difference may be attributed to the fact that they investigated the collision process in a biased configuration, that is, onto a two-dimensional ordered packing.

A careful analysis of the vertical speed distributions shows that the most likely value is on the order of $2\sqrt{gd}$ and is relatively insensitive to a variation of the impact angle from 10° to 90° . On the contrary, it increases slightly with increasing impact velocity. These features can also be clearly observed through the mean vertical ejection speed \bar{V}_z (see Fig. 9). The increase of \bar{V}_z with increasing impact speed, although weak, is measurable and can be described by a power law:

$$\frac{\bar{V}_z}{\sqrt{gd}} \approx 1.06 \left(\frac{V_i}{\sqrt{gd}} \right)^{1/4}. \quad (19)$$

The mean quadratic vertical velocity is, as well, slightly increasing with increasing impact velocity, and can be approximated by

$$\frac{\bar{V}_z^2}{gd} \approx 1.46 \left(\frac{V_i}{\sqrt{gd}} \right)^{1/2}. \quad (20)$$

At this stage, we would like to stress that the variation of the mean quadratic vertical ejection speed with the impact velocity is in agreement with the previous results. Let us recall that $E_{tot,z}$ was found to be proportional to $(1 - e_{xz}^2)E_i$. Using the fact that $E_{tot,z} = m\bar{n}_{ej}\bar{V}_z^2/2$ and taking advantage of Eq. (15), one can derive an expression for \bar{V}_z^2 :

$$\frac{\bar{V}_z^2}{gd} = \frac{r_z(1 - e_{xz}^2)}{\bar{n}_{ej}} \frac{V_i^2}{gd} \approx 1.5 \left(\frac{V_i}{\sqrt{gd}} \right)^\alpha, \quad (21)$$

with $\alpha \approx 0.5$. This result is very close to that extracted directly from the velocity distributions [cf. Eq. (20)].

Let us turn now to the distributions of the horizontal ejection velocities. They are surprisingly almost symmetrical [see Figs. 8(c) and 8(d)]. For an impact angle of 90° , the distribution is symmetrical with a zero mean (as expected) and can be well approximated by a normal distribution law. For impact angles smaller than 90° , a slight asymmetry appears and the distribution is off centered (the most likely value of the distribution is shifted along the positive axis). However, the distribution can still be reasonably approximated by a normal law with a nonzero mean value:

$$P[\tilde{V}_x] = \frac{1}{\sqrt{2\pi}s} \exp[-(\tilde{V}_x - m)^2/2s^2]. \quad (22)$$

We set $\tilde{V}_x = V_x/\sqrt{gd}$. The parameters m and s are, respectively, the mean and the root mean square of the horizontal velocity (i.e., $m = \bar{V}_x$ and $s^2 = \overline{V_x^2} - \bar{V}_x^2$), and are given in Table II. The dependence of the mean value of the horizontal velocity (as well as the mean quadratic value) on the impact velocity and impact angle is shown in Fig. 9. The mean velocity \bar{V}_x is rather independent of the impact velocity, but decreases with increasing impact angle (it vanishes for normal impact). It can be relatively well fitted by a cosine function of θ_i :

$$\frac{\bar{V}_x}{\sqrt{gd}} \approx 0.65 \cos \theta_i. \quad (23)$$

Finally, the mean quadratic velocity is independent of both the impact velocity and impact angle: $\overline{V_x^2}/gd \approx 3-4$.

D. Distribution of the 2D ejection angle θ and 2D ejection speed V_{xz}

We also determined the probability distribution function $P(\theta)$ of the 2D ejection angle of the splashed particles [defined as $\theta = \arctan(V_z/V_x)$] for various impact velocities and impact angles (see Fig. 10). The distribution function $P(\theta)$ is almost insensitive to the impact velocity. At an impact angle of 10° , the mean ejection angle $\bar{\theta}$ remains constant and is on the order of 80° for a large range of impact speeds [see Fig. 11(a)]. On the contrary, it increases with increasing impact angles and reaches the value of 90° for normal impacts, as expected due to symmetry [see Fig. 11(b)]. The variation of

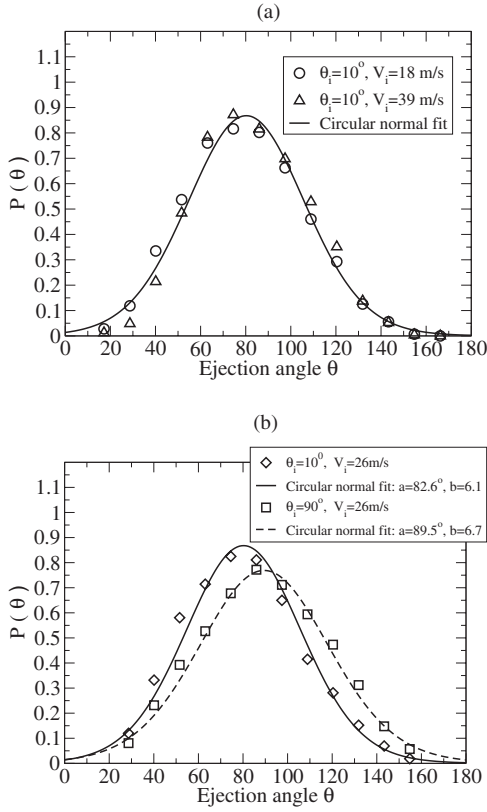


FIG. 10. Distribution of the ejection angle θ (deg) (a) for various impact speeds at a fixed impact angle of 10° ; (b) for various impact angles at a fixed impact velocity of 26 m/s. The continuous lines stand for the corresponding Von Mises distributions.

$\bar{\theta}$ with the impact angle can be approximated by a linear law of the form

$$\bar{\theta} = \frac{\pi}{2} + 0.1 \left(\theta_i - \frac{\pi}{2} \right), \quad (24)$$

where θ_i is expressed in radians.

The distribution function $P(\theta)$ can be approximated with good accuracy by a Von Mises distribution (also known as circular normal distribution):

$$P(\theta) = \frac{e^{b \cos(\theta-a)}}{2\pi I_0(b)}, \quad (25)$$

where I_0 is the modified Bessel function of the first kind of order 0. The mean value of the distribution is a and the circular variance is $1 - (\cos \theta)^2 - (\sin \theta)^2 = 1 - I_1(b)/I_0(b)$. The values of a and b for various impact parameters are given in Table III.

Lastly, we examined the distribution of the 2D ejection speed V_{xz} defined as $V_{xz} = \sqrt{V_x^2 + V_z^2}$ (see Fig. 12). V_{xz} follows the same trends as the vertical ejection speed V_z . The distribution $P(V_{xz})$ is well approximated by a log-normal distribution [cf. Eq. (16)]. The mean μ and variance σ of the distribution of $\ln[(V_{xz} - V_0)/\sqrt{gd}]$ are given in Table III. The mean ejection speed is insensitive to the impact speed but slightly increases with increasing impact speed (see Fig. 13). As for

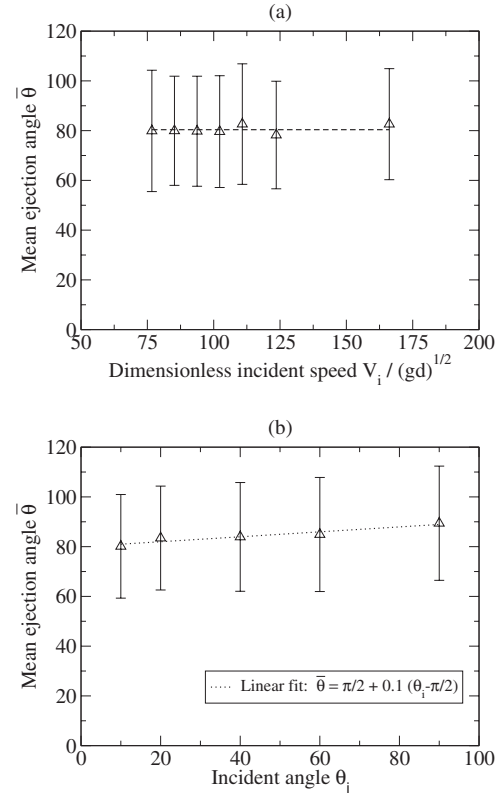


FIG. 11. Mean ejection angle (deg) (a) versus the impact speed at a fixed impact angle of 10° ; (b) versus the impact angle at a fixed impact velocity of 26 m/s. In (a), the dashed line represents an average of the data, while in (b) the dotted line stands for a linear fit [cf. Eq. (24)]. Note that the error bars represent the root mean square of the angular distributions.

the vertical ejection speed, the variation of \bar{V}_{xz} and $\overline{V_{xz}^2}$ with the impact speed can be approximated by a power law of V_i :

$$\frac{\bar{V}_{xz}}{\sqrt{gd}} \approx 1.18 \left(\frac{V_i}{\sqrt{gd}} \right)^{1/4}, \quad (26)$$

$$\frac{\overline{V_{xz}^2}}{gd} \approx 1.84 \left(\frac{V_i}{\sqrt{gd}} \right)^{1/2}. \quad (27)$$

This result supports reasonably well the numerical predictions of Anderson and Haff [14] who found that $\bar{V}_{xz} \sim V_i^{0.3}$ [cf. Eq. (7)]. Note also that the scaling found for the mean quadratic ejection velocity V_{xz} is compatible with the fact that the total kinetic energy $E_{tot,xz}$ of the splashed particles varies as V_i^2 , recalling that the mean number \bar{n}_{ej} of ejected particles scales as $V_i^{3/2}$ ($E_{tot,xz} \sim \bar{n}_{ej} \overline{V_{xz}^2} \sim V_i^2$).

E. Correlation analysis

In order to extract from our data the bivariate distribution $P(V_x, V_z)$ of the ejection velocity, it is necessary to investigate whether the components V_x and V_z of a splashed particle are correlated or not. The correlation coefficient ρ between two variables V_1 and V_2 is usually defined as

TABLE III. Main features of the distributions of the ejection angle θ and ejection speed V_{xz} , for various impact speeds at a fixed impact angle of 10° and for various impact angles at a fixed impact velocity $V_i=26$ m/s. The parameter s corresponds to the root mean of the ejection angle and b is the parameter of the Von Mises distribution, whereas μ and σ are the parameters of the log-normal distribution of $(V_{xz}-V_0)/\sqrt{gd}$.

V_i (m/s)	$\bar{\theta}=a$	s	b	\bar{V}_{xz}/\sqrt{gd}	$\overline{V_{xz}^2}/gd$	μ	σ
18	79.9	24.4	6.0	3.57	16.65	0.47	0.78
20	79.9	21.9	7.3	3.57	16.73	0.46	0.79
22	79.8	22.1	7.2	3.57	17.04	0.45	0.80
24	79.6	22.5	7.0	3.62	17.13	0.49	0.78
26	82.6	24.2	6.1	3.81	19.02	0.59	0.76
29	78.2	21.6	7.5	3.98	20.37	0.68	0.73
39	82.6	22.3	7.1	4.17	23.73	0.71	0.78
θ_i	$\bar{\theta}=a$	s	b	\bar{V}_{xz}/\sqrt{gd}	$\overline{V_{xz}^2}/gd$	μ	σ
10°	82.6	24.2	6.1	3.81	19.02	0.59	0.76
20°	83.5	20.9	8.0	3.55	15.01	0.55	0.65
40°	84.0	20.8	7.3	3.50	14.31	0.55	0.61
60°	84.9	22.9	6.7	3.71	16.07	0.65	0.60
90°	89.5	22.9	6.7	3.42	13.42	0.51	0.60

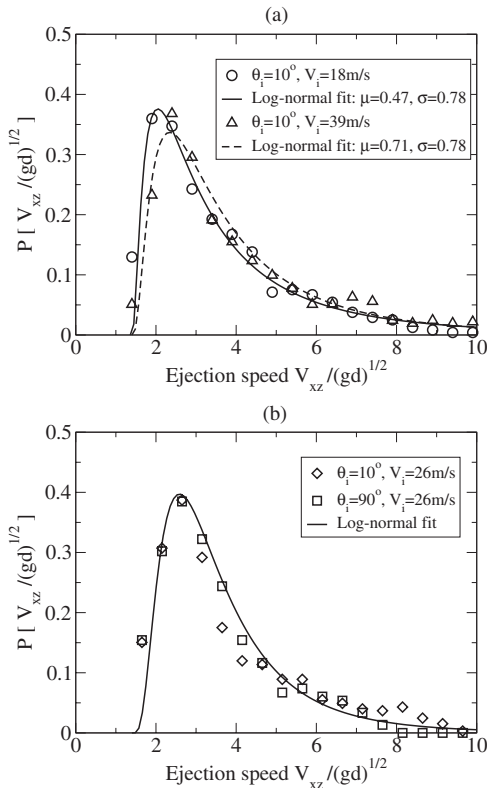


FIG. 12. Distribution of the 2D ejection speed V_{xz} (a) for various impact angles at a fixed impact velocity of 26 m/s; (b) for various impact speeds at a fixed impact angle of 10° . The continuous lines represent the corresponding log-normal distributions.

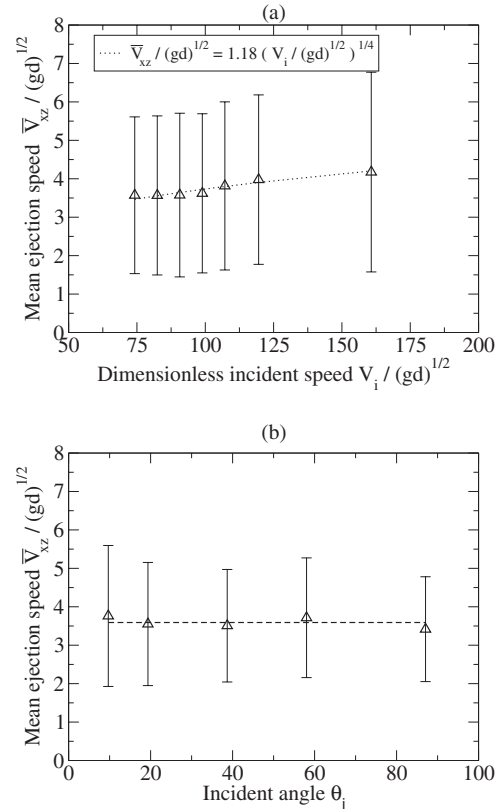


FIG. 13. Mean ejection speed \bar{V}_{xz} (a) versus the impact speed at a fixed impact angle of 10° (the dashed line represents a power law fit $V_i^{1/4}$); (b) versus the impact angle at a fixed impact velocity of 26 m/s (the horizontal line corresponds to an average of the data).

$$\rho(V_1, V_2) = \frac{\overline{V_1 V_2} - m_1 m_2}{s_1 s_2} \quad (28)$$

where m_1 (m_2) and s_1^2 (s_2^2) are the mean and the variance of V_1 (V_2). We calculated the correlation coefficient between V_x and V_z for various impact parameters (see Fig. 14). At grazing impacts, the correlation coefficient is rather large (greater than 0.5) for moderate impact speeds and decreases with increasing impact speed (down to 0.3 for $V_i=161\sqrt{gd}$). In addition, the correlation coefficient vanishes for normal impacts, as expected. V_x and V_z are therefore strongly correlated, except for normal impacts. The existence of this correlation is in fact not surprising, since we have seen that the splashed particles are ejected with a preferential angle. As a consequence, it is not legitimate to approximate the bivariate probability distribution $P(V_x, V_z)$ by the product of $P(V_x)$ and $P(V_z)$.

Alternatively, we can wonder whether the 2D ejection speed V_{xz} and ejection angle θ are correlated. The correlation $\rho(V_{xz}, \theta)$ between V_{xz} and θ follows the same trends as the correlation between V_x and V_z (see Fig. 14). However, $\rho(V_{xz}, \theta)$ appears to be much less important. For impact speeds greater than $100\sqrt{gd}$, it is always smaller than 0.2. It is therefore tempting to assume, in a first approximation, that V_{xz} and θ are uncorrelated variables. In the next section, we will show indeed that the bivariate probability distribution

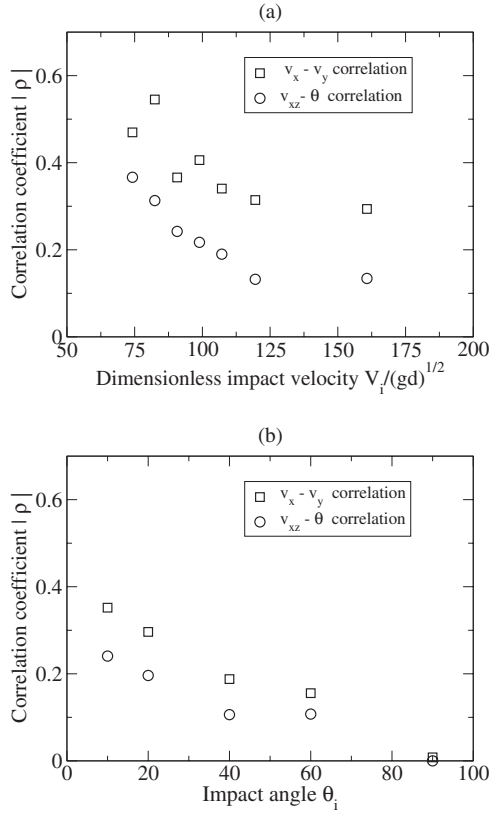


FIG. 14. Correlation between V_x and V_z and between V_{xz} and θ for various impact parameters: (a) at a fixed impact angle of 10° for various impact speeds; (b) at a fixed impact speed of 26 m/s for various impact angles.

$P(V_x, V_z)$ can be very well approximated by the product of $P(V_{xz})$ and $P(\theta)$.

F. Bivariate distribution of the ejection speed of the splashed particles

As seen previously, the variables V_{xz} and θ characterizing the ejection speed of the splashed particles can be, as a first approximation, considered as uncorrelated variables. The bivariate distribution $P(V_{xz}, \theta)$ can therefore be approximated by the product of the univariate distributions $P(V_{xz})$ and $P(\theta)$:

$$P(\tilde{V}_{xz}, \theta) = \frac{\exp\{-[\ln(\tilde{V} - \tilde{V}_0) - \mu]^2/2\sigma^2\}}{\sqrt{2\pi}\sigma(\tilde{V} - \tilde{V}_0)} \times \frac{\exp[b \cos(\theta - a)]}{2\pi I_0(b)}. \quad (29)$$

Note that the bivariate distribution is normalized so that $\int_0^\pi d\theta \int_{\tilde{V}_0}^\infty dV P(V, \theta) = 1$. The normalized bivariate distribution $P(V_x, V_z)$ is simply deduced from $P(V_{xz}, \theta)$ by the following relation:

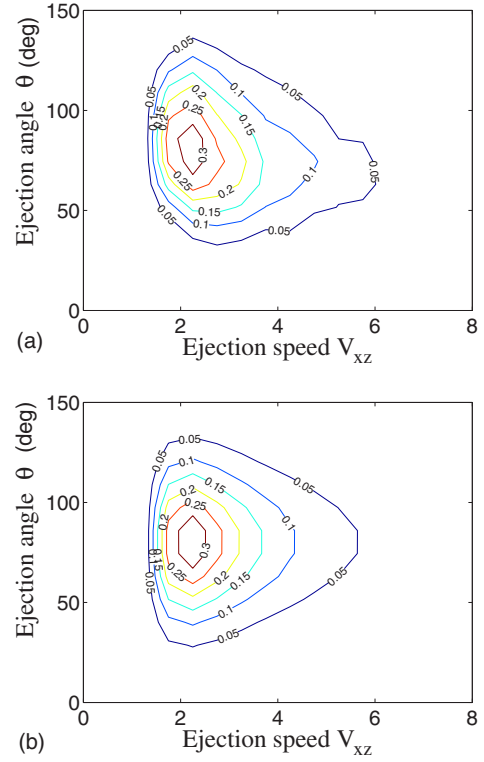


FIG. 15. (Color online) Isoprobability lines of the bivariate distribution $P(V_{xz}, \theta)$ for an impact angle of 10° and an impact speed of 22 m/s (i.e., $94\sqrt{gd}$): (a) experimental data; (b) prediction obtained from Eq. (29).

$$P(V_x, V_z) = \frac{P(V_{xz}, \theta)}{V_{xz}}, \quad (30)$$

such as $\int_{-\infty}^\infty dV_x \int_{V_0}^\infty dV_z P(V_x, V_z) = 1$. In Fig. 15, we compared the isoprobability lines of the bivariate distribution $P(V_{xz}, \theta)$ extracted from the experimental data and that calculated from Eq. (29). The agreement is remarkably good and confirms that the approximation considering V_{xz} and θ as uncorrelated variables is fairly good.

VI. SUMMARY AND CONCLUSION

We characterized experimentally in an extensive way the collision of an incident spherical particle against a 3D granular packing of identical particles. We provided a full description of the splash function in the incident plane for a wide range of impact velocities (from $50\sqrt{gd}$ to $200\sqrt{gd}$) and impact angles (from 10° to 90°). The main striking results can be summarized as follows.

(i) We showed that the impacting particle loses much more energy for head-on impacts than for grazing collisions. In other words, the effective restitution coefficient e_{xz} for the incident particle decreases with increasing impact angle: $\bar{e}_{xz} \approx 0.87 - 0.72 \sin \theta_i$.

(ii) In counterpart, more beads are ejected from the bed for normal impacts. We indeed demonstrated that, at a fixed impact speed, the mean number of ejected grains is propor-

tional to the fraction of incident kinetic energy $(1 - e_{xz}^2)$ communicated to the packing.

(iii) An increase of the impact speed mainly results in an augmentation of the number of ejected beads ($\bar{n}_{ej} \sim V_i^{3/2}$), the mean kinetic energy of the splashed particles being only weakly affected ($\bar{V}_{xz}^2 \sim V_i^{1/2}$).

(iv) The variation of the mean number of splashed particles with the impact angle and speed can be cast into the simple following law: $\bar{n}_{ej} \approx 0.02(1 - e_{xz}^2)V_i^{3/2}$.

(v) The sum of the kinetic energy $E_{tot,xz}$ of the splashed beads is found to be proportional to the energy communicated to the packing: $E_{tot,xz} \approx m\bar{n}_{ej}\bar{V}_{xz}^2 \approx 0.038(1 - e_{xz}^2)E_i$. This result is a direct consequence of the scaling of \bar{n}_{ej} and \bar{V}_{xz}^2 with the impact speed V_i .

(vi) We also showed that the distribution of the vertical ejection speeds can be well approximated by a log-normal distribution; the mean value was found to be independent of the impact angle and to vary weakly with the impacting speed: $\bar{V}_z/\sqrt{gd} \approx 1.06(V_i/\sqrt{gd})^{1/4}$.

(vii) The distribution of the horizontal ejection speed is nearly Gaussian with a nonzero mean except for head-on impacts: $\bar{V}_x/\sqrt{gd} \approx 0.65 \cos \theta_i$.

(viii) The vertical and horizontal ejection speeds were found to be strongly correlated due to the fact the splashed particles are ejected with a preferential angle. As a consequence, the bivariate distribution $P(V_x, V_z)$ cannot be approximated by the product of the univariate distributions $P(V_x)$ and $P(V_z)$.

(ix) On the contrary, the norm V_{xz} of the ejection speed and the ejection angle θ are weakly correlated. The bivariate

distribution $P(V_{xz}, \theta)$ is therefore very well approximated by the product of the univariate distributions $P(V_{xz})$ and $P(\theta)$, which were found to follow, respectively, a log-normal law and a normal circular distribution.

(x) Lastly, the mean ejection velocity V_{xz} was shown to behave similarly to the mean vertical ejection speed [$\bar{V}_{xz}/\sqrt{gd} \approx 1.18(V_i/\sqrt{gd})^{1/4}$], whereas the mean ejection angle θ was found to be dependent only on the impact angle: $\bar{\theta} = \pi/2 + 0.1(\theta_i - \pi/2)$.

These outcomes, which comprise a rather complete and accurate description of the 2D splash function for a wide range of impact parameters, should provide valuable and useful pieces of information to be implemented in numerical and/or analytical models of eolian sand transport. In the near future, we plan to give a full 3D description of the splash function, and in particular to characterize the dispersion of the ejected particles in the direction perpendicular to the incident plane. This is an important issue in the context of eolian sand transport if one desires to quantify the coupling between the longitudinal and transverse sand transport.

ACKNOWLEDGMENTS

This work was supported by a grant from the French Ministry of Research (ACI Grant No. 500270). We would like also to thank J. T. Jenkins and J. M. Pasini for stimulating discussions and critical readings of the manuscript. Moreover, A.V. is grateful to G. Le Cäer for his valuable advice concerning the statistical description of the experimental data.

-
- [1] R. A. Bagnold, *The Physics of Blown Sand and Desert Dunes* (Chapmann and Hall Methuen, London, 1941).
- [2] R. S. Anderson, M. Sorensen, and B. B. Willets, *Acta Mech. (Suppl.)* **1**, 1 (1991).
- [3] B. B. Willets and M. A. Rice, *Acta Mech.* **63**, 255 (1986).
- [4] S. Mitha, M. Q. Tran, B. T. Werner, and P. K. Haff, *Acta Mech.* **63**, 267 (1986).
- [5] B. T. Werner, *J. Geol.* **98**, 1 (1990).
- [6] S. Denisov, J. Klafter, and M. Urbakh, *Phys. Rev. Lett.* **91**, 194301 (2003).
- [7] A. M. Walsh, K. E. Holloway, P. Habdas, and J. R. de Bruyn, *Phys. Rev. Lett.* **91**, 104301 (2003).
- [8] Y. Grasseli and H. Herrmann, *Granular Matter* **3**, 201 (2001).
- [9] F. Rioual, A. Valance, and D. Bideau, *Phys. Rev. E* **62**, 2450 (2000).
- [10] F. Rioual, Ph.D. thesis, Université de Rennes 1, 2002 (unpublished).
- [11] F. Rioual, A. Valance, and D. Bideau, *Europhys. Lett.* **61**, 194 (2003).
- [12] B. T. Werner and P. K. Haff, *Sedimentology* **35**, 189 (1988).
- [13] R. S. Anderson and P. K. Haff, *Science* **241**, 820 (1988).
- [14] R. S. Anderson and P. K. Haff, *Acta Mech. (Suppl.)* **1**, 21 (1991).
- [15] L. Oger, A. V. M. Ammi, and D. Beladjine, *Eur. Phys. J. E* **17**, 467 (2006).
- [16] B. R. White and J. C. Schulz, *J. Fluid Mech.* **81**, 497 (1977).
- [17] R. S. Anderson and B. Hallet, *Geol. Soc. Am. Bull.* **97**, 523 (1986).